# A new explanation of the sawtooth phenomena in tokamaks 🅵 ⓢⓒ🅸

ⓘ S. C. Jardin, ⓘ I. Krebs and ⓘ N. Ferraro

## COLLECTIONS

🅵    This paper was selected as Featured

ⓢⓒ🅸    This paper was selected as Scilight

🌐        ⬆️        🔴

View Online      Export Citation      CrossMark

## ARTICLES YOU MAY BE INTERESTED IN

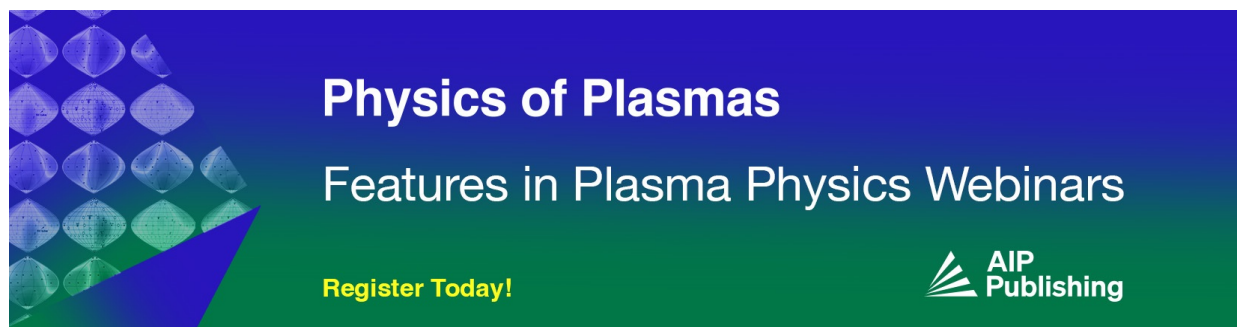Mechanisms of energetic-particle transport in magnetically confined plasmas
Physics of Plasmas **27**, 030901 (2020); https://doi.org/10.1063/1.5136237

Role of sheared E × B flow in self-organized, improved confinement states in magnetized plasmas
Physics of Plasmas **27**, 060501 (2020); https://doi.org/10.1063/1.5142734

Machine learning control for disruption and tearing mode avoidance
Physics of Plasmas **27**, 022501 (2020); https://doi.org/10.1063/1.5125581

**Physics of Plasmas**

Features in Plasma Physics Webinars

**Register Today!**

AIP Publishing

# A new explanation of the sawtooth phenomena in tokamaks

S. C. Jardin,[1,a)] I. Krebs,[2] and N. Ferraro[1]

**AFFILIATIONS**

[1]Princeton Plasma Physics Laboratory, P.O. Box 451, Princeton, New Jersey 08543, USA
[2]Dutch Institute for Fundamental Energy Research, De Zaale 20, Eindhoven 5612 AJ, The Netherlands

**Note:** This paper is part of the Special Collection: Papers from the 61st Annual Meeting of the APS Division of Plasma Physics.
[a)]Author to whom correspondence should be addressed: jardin@pppl.gov

**ABSTRACT**

The ubiquitous sawtooth phenomena in tokamaks are so named because the central temperature rises slowly and falls rapidly, similar to the blades of a saw. First discovered in 1974, it has so far eluded a theoretical explanation that is widely accepted and consistent with experimental observations. We propose here a new theory for the sawtooth phenomena in auxiliary heated tokamaks, which is motivated by our recent understanding of "magnetic flux pumping." In this theory, the role of the $(m, n) = (1, 1)$ mode is to generate a dynamo voltage, which keeps the central safety factor, $q_0$, just above 1.0 with low central magnetic shear. When central heating is present, the temperature on axis will increase until at some point, and the configuration abruptly becomes unstable to ideal MHD interchange modes with equal poloidal and toroidal mode numbers, $m = n > 1$. It is these higher order modes and the localized magnetic stochasticity they produce that cause the sudden crash of the temperature profile, not magnetic reconnection. Long time 3D MHD simulations demonstrate these phenomena, which appear to be consistent with many experimental observations.

*Published under license by AIP Publishing.* https://doi.org/10.1063/1.5140968

## I. INTRODUCTION

Typical tokamak discharges undergo "sawtooth" cycles in which the central temperature periodically peaks until a rapid onset instability causes the temperature near the center to suddenly flatten, and then this process repeats. This phenomenon was first observed in 1974[1] and has since been regularly observed in all tokamaks on many diagnostics including soft x-ray, temperature, and density measurements.

Forty-five years after its discovery, there is still no widely accepted theory for the sawtooth phenomenon, which is consistent with experimental observations. Such theories are needed to construct accurate numerical models, which predict such things as transport near the magnetic axis in whole-device-modeling codes,[2] excitation of neoclassical tearing modes,[3] and central accumulation of heavy metal impurities in future tokamaks.[4]

The two leading existing theories, described in Sec. II, are incomplete and are at odds with many experimental measurements. In this paper, we describe a new theory for sawtooth oscillations that may occur in some discharges. The mechanism for these oscillations was determined by performing many long-time 3D extended magnetohydrodynamic (XMHD) simulations with the M3D-C1 code.[5] The

advantage of a simulation over an experiment is that it can be diagnosed to arbitrary precision. The disadvantage, of course, is that the equations being solved are an incomplete description of reality. Therefore, we present this as a "new theory" and not an absolute proof of the mechanism behind this phenomenon. We hope that this new theory will be considered as an alternative possibility when interpreting experimental results.

In Sec. II, we discuss the two leading existing theories for the sawtooth oscillation, namely, the Kadomtsev model and the Wesson model, and why they are incomplete and/or inconsistent with many experimental results. Section III describes the main features of the new model being proposed here and how it relates to the Wesson model. In Sec. IV, we present the results from a long-time M3D-C1 simulation in which sawteeth are observed. Section V presents a simple model that illustrates what the motional Stark effect (MSE) magnetic signature of the new model of the sawtooth would look like. In Sec. VI, we review some of the literature on experimental measurements of the central safety factor before and after the sawtooth crash. This is the major discriminator between different models. We also make recommendations for future work. Finally, we present our conclusions in Sec. VII.

## II. LEADING THEORETICAL MODELS

There are two leading models of the sawtooth in tokamaks, which we will call the Kadomtsev model and the Wesson model. The Kadomtsev model involves magnetic reconnection, but the Wesson model does not. We briefly describe these and some of their confirmations and limitations.

### A. The Kadomtsev model

The interpretation of sawtooth oscillations has been strongly affected by a seminal paper by Kadomtsev in 1975.[6] In his model, the central safety factor, $q_0$, continues to drop from value 1 due to current peaking in a discharge with centrally peaked temperature and Spitzer-like resistivity. At some point, when $q_0$ is low enough, a $(m, n) = (1, 1)$ (where $m$ and $n$ are poloidal and toroidal mode numbers) resistive reconnection event occurs, flattening the temperature and density profiles interior to the $q = 1$ surface and returning $q_0$ to 1. This process has been shown to occur in 3D resistive MHD and 2-fluid MHD simulations[5,7–12] for tokamaks with sufficiently low values of pressure or $\beta = 2\mu_0 \langle p \rangle / B^2$: $\beta \ll 1$ and/or sufficiently low values of the Lundquist number $S = \tau_R / \tau_A < 10^5$, where $\tau_R$ and $\tau_A$ are the resistive diffusion time and Alfvén transit time, respectively. However, these low-$\beta$, low temperature simulations do not exhibit the fast, ideal MHD time scale, temperature drops during the sawtooth cycle, which are observed experimentally.[13] We also note that some of these calculations included unphysical current sources, and some are now thought to be inadequately resolved in the toroidal direction.[14]

Influenced by the Kadomtsev model, the fast temperature drops observed in many experiments have almost universally been assumed to be caused by *fast magnetic reconnection*, and a number of numerical studies have been published reporting to observe this fast reconnection in the simulation of a sawtooth event caused either by anomalous electron viscosity,[15] two-fluid effects,[16–18] high-n ballooning modes,[19] plasmoids,[20] or plasma compressibility.[21] However, a common feature of these studies is that they only simulate a single sawtooth event, and the initial conditions are such that the central safety factor is much less than unity so that the configuration is strongly unstable from the beginning of the simulation. An obvious question is, "How did the plasma get into this unstable state, which was used to initialize the calculation?"

In our resistive MHD simulations, we only observe Kadomtsev reconnection events at low values of the Lundquist number, $S$, and at low $\beta$, such as that existed in the ST tokamak in which sawtooth oscillations were originally observed. It is well known that a collisional tokamak plasma is unstable to a (1,1) resistive kink MHD instability whenever $q_0 < 1$. The growth rate of this instability scales as a fractional power of the resistivity, $\gamma \sim \eta^{1/3} \sim S^{-1/3}$,[22] whereas the rate that $q_0$ decreases due to resistive diffusion is much slower, $\tau_R^{-1} \sim \eta \sim S^{-1}$.[23] Although in reality this mode will be modified by FLR and other kinetic effects,[24] the scaling $\gamma\tau_R \sim \eta^{-2/3} \sim S^{2/3}$ makes it unlikely that $q_0$ could ever be substantially below 1, at least in a self-consistent resistive MHD simulation at high $S$.

### B. The Wesson model

An alternative to the Kadomtsev model is the pressure driven interchange model first put forth by Wesson[25,26] in cylindrical geometry and soon afterward extended to toroidal geometry.[27,28] Wesson noted that if the central safety factor was above but very close to unity in a region near the magnetic axis, $|1 - q| \ll 1$, the configuration could become unstable to an ideal MHD (1, 1) interchange instability that could flatten the temperature profiles on an ideal MHD time scale without substantially changing the magnetic field. The fact that the stability of this very low shear configuration is strongly affected by small changes in the $q$-profile can potentially explain the sudden onset of the crash. The Wesson model, which does not involve magnetic reconnection, did much to explain the fast crash times, but it was incomplete in that it did not explain why the central $q$-profile remained close to 1 over an extended region in the presence of resistive diffusion, and it did not explicitly state what caused the onset of the crash.

## III. THE NEW MODEL

The new sawtooth model being proposed here is really an extension of the Wesson model and builds on his insight. We propose that the $q$-profiles is very near, and slightly above, 1 in a region near the magnetic axis of the tokamak, and that it does not appreciably change during the sawtooth cycle. This is in agreement with the Wesson model. However, in our model, the (1, 1) mode is not responsible for the crash phase of the sawtooth. Rather, it nonlinearly saturates at a low amplitude and produces a central loop voltage through the dynamo effect that keeps $q_0$ from falling below 1. The crash occurs when other ideal MHD interchange modes $(m, n)$ with $m = n > 1$ become unstable causing a localized stochastic region to form near the magnetic axis. We next discuss each of these phenomena separately.

### A. The saturated (1, 1) mode

Recent papers by us[11,29] reported on long time self-consistent simulations where we demonstrated that a pressure driven (1, 1) interchange mode will be unstable in a tokamak with $q_0$ just above 1 with low central shear, much as predicted by Wesson and others. However, we found that the mode saturates nonlinearly at a fairly small amplitude. In those papers, we focused on how "magnetic flux pumping" could explain sawtooth-free "hybrid" discharges[30–34] and "long lived modes."[35–37] The basic mechanism is that for a sufficiently low central magnetic shear discharge with $q_0 \gtrsim 1$, any pressure gradient will cause a $(n, m) = (1, 1)$ interchange instability to develop. This (1, 1) interchange mode nonlinearly produces a central (0, 0) dynamo loop voltage that acts to raise $q_0$. If the pressure gradient exceeds a critical value, the resulting dynamo loop voltage will be strong enough to keep $q_0 \gtrsim 1$. Since, as shown in the Appendix, the growth rate for this (1, 1) mode, which creates the dynamo voltage, is a maximum at $q_0 = 1$ and decreases as $q_0$ increases further,[27,28] this serves to regulate the process and keeps $q_0 \gtrsim 1$.

### B. The (n,n) modes with n > 1

However, what if sufficient central heating is applied to keep peaking the temperature and density profiles despite the (1, 1) velocity field from the interchange mode acting to flatten them? The profiles will then continue to peak until some other instability sets in. We find that there is a critical pressure gradient, or peaking, for which many high-n modes with $m = n$ abruptly become unstable, causing a stochastic region to form near the magnetic axis, locally flattening the profiles in the center. This process does not involve magnetic reconnection as the $q$-profile remains slightly above unity and nearly

shear-free, and the modes are non-resonant. In this picture, the role of the $(1, 1)$ mode is to regulate the $q$-profile, and it is the $(m, n)$ modes with $m = n > 1$, which are responsible for the crash phase. This is consistent with ideal MHD analysis by Kirby[38] of cylindrical equilibria with a flat central $q$-profile with $q_0$ just slightly above unity: the higher $n$ modes with $n = m$ can have higher growth rates than the $(1, 1)$ mode, although their instability region in $(q_0, \beta_{p1})$ space is smaller.

We have extended Kirby's numerical results to toroidal geometry and find qualitatively similar results, which were also found analytically.[27,28] Figure 1 shows linear stability boundaries for the first eight toroidal modes for a set of model toroidal equilibria with a circular cross section, aspect ratio $R/a = 3.2$, pressure, and safety factor profiles given by

$$p = p_0 \times (1 - \tilde{\psi})^2, \tag{1}$$

$$q = \begin{cases} q_0 & \text{if } \tilde{\psi} \leq \psi_1 \\ q_0 + q_1(\tilde{\psi} - \psi_1)^2 & \text{if } \tilde{\psi} > \psi_1. \end{cases} \tag{2}$$

Here, $\tilde{\psi}$ is the normalized poloidal flux, $\psi_1 = 0.2$, $q_1 = 3.5322$. The horizontal axis in Fig. 1 is given by $\beta_{p1} \equiv \mu_0 \int_0^{\psi_1} [p(\psi) - p_1] dV / \int_0^{\psi_1} \frac{1}{2} B_p^2 dV$, where $p_1$ is the value of $p$ at $\psi_1$. Figure 2 gives the linear growth rates vs $q_0$ along the dotted line in Fig. 1 with $\beta_{p1} = 0.531$. Figure 3 shows the mode structure for a typical $(4, 4)$ mode as an illustration. It is seen that the mode is confined to the inner magnetic shear-free region of the cross section.

The equilibria in the upper left corner of Fig. 1 are stable to all ideal MHD modes. As $q_0$ is lowered toward 1 and/or the pressure is increased so that $\beta_{p1}$ increases, we move down and/or to the right in the diagram. When the black line is crossed, the $(1, 1)$ mode sets in, which causes the dynamo voltage described in the Appendix to develop and stop the decrease in $q_0$. If the pressure is further increased and the green line is crossed, an ideal MHD $(2, 2)$ mode will become unstable. This will likely destabilize $(3, 3)$, $(4, 4)$, etc. modes through
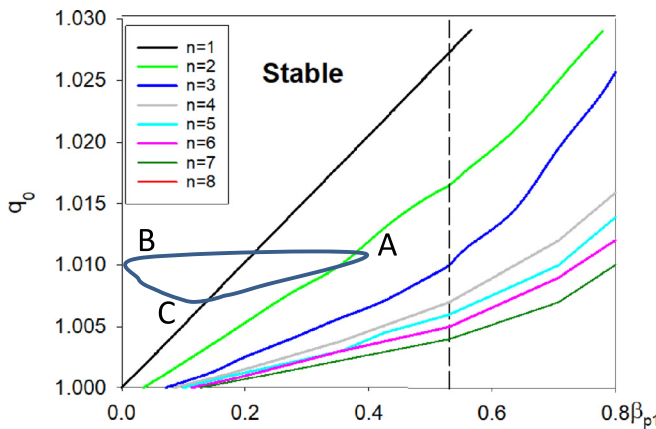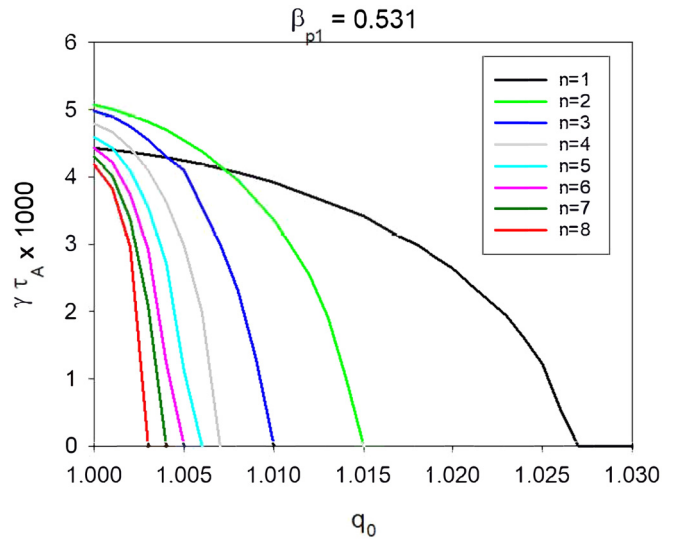


**FIG. 2.** Growth rates for modes $(n, n)$ for $n = 1 - 8$ along the dotted line in Fig. 1 with $\beta_{p1} = 0.531$.

nonlinear mode coupling, causing the center region to become stochastic and hence the sawtooth crash.

## IV. M3D-C1 SIMULATION RESULTS

Here, we report on a 3D MHD simulation of multiple sawteeth occurring in a tokamak plasma with moderate $\beta$. We employ a modern, massively parallel, implicit 3D MHD code, which uses high-order finite elements in all three dimensions.[5] These features enable high-resolution and long timescale calculations of MHD activity in a tokamak. Unlike the papers cited in Sec. II A, we do not start the
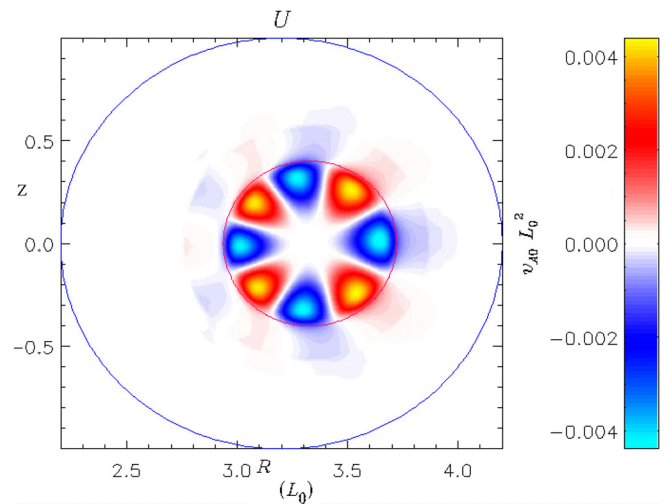


**FIG. 1.** Typical sawtooth cycle in $q_0, \beta_{p1}$ space. (a) Crash occurs when entering the $(n, n)$ unstable regime with $n > 1$. (b) Crash causes $\beta_{p1}$ to drop, but $q_0$ is largely unchanged. $q_0$ then begins to drop due to resistive diffusion as $\beta_{p1}$ increases due to external heating. (c) Crossing the $(1, 1)$ stability boundary causes $q_0$ to increase due to dynamo voltage as $\beta_{p1}$ continues to rise until the $n > 1$ stability boundary is crossed.



**FIG. 3.** Velocity stream function for the $(4, 4)$ mode with $(q_0, \beta_{pq}) = (1.005, 0.531)$ for the profiles given in Eqs. (1) and (2). Also shown is the $q = 1.01$ surface. Note that the mode is confined to the shear-free region. The mode structure for the other modes is very similar but with differing periodicity.
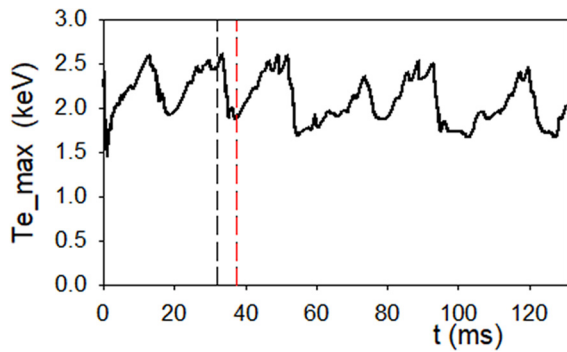
**FIG. 4.** Maximum electron temperature vs time in a long-time M3D-C1 simulation of an auxiliary heated tokamak plasma. In normalized units, this simulation ran for 500,000 $\tau_A$.

configuration in an unstable state and watch its transition into a stable state. Rather, we define particle and energy sources and transport coefficients and run for 100's of 1000's of Alfvén times and look for a repeating cycle.

## A. Sawtoothing simulation

We show the results in Figs. 4–6 of a M3D-C1 simulation of a canonical tokamak discharge with aspect ratio $R/a = 3.2$, ellipticity $\kappa = 1.3$, triangularity $\delta = 0.2$, $\beta \gtrsim 2\%$, and edge safety factor $q_a = 4.3$. Figure 4 shows that the simulation develops quasi-periodic oscillations in which the central temperature slowly rises and abruptly crashes, as is the case in sawtooth oscillations. Consistent with the new model described above, in this simulation, $q_0$ never falls below unity, and the oscillations and fast crashes are not primarily due to the (1, 1) mode. At the start of each temperature crash, a large number of localized $(m, n)$ modes with $m = n > 1$ grow up and cause only the central region to become stochastic.

Shown in Fig. 5(left) is the midplane temperature profile just before and just after a crash at the times indicated by the vertical lines in Fig. 4. The central electron temperature is seen to have decreased by about 25% during the crash. Not shown is that the central density also decreased but only slightly, presumably because it is originally less peaked than the temperature due to the lack of central fueling and because the density equation does not contain a large parallel diffusion term. Shown on the right are the $q$-profiles at the same two times, which are seen to stay essentially unchanged. Also shown in the two graphs, in dashed lines, are the results we obtained in a 2D axisymmetric calculation with the same transport coefficients and heating sources. Of course, there is no (1, 1) mode activity and no crashes in 2D, and the central temperatures are higher and the $q$-profile is lower because of this.

We show Poincaré plots at the same two time slices in Fig. 6. It is seen that before the crash, the magnetic surfaces are mostly good everywhere, with some small islands at rational surfaces. Just after the crash, most of the surfaces are still good, but those near the center have been destroyed. Both the $E \times B$ convective velocities from the many unstable modes and parallel transport in the stochastic region contribute to the temperature flattening.

Figure 7 is a closeup of one of the "crash" periods, delineated with dashed vertical lines in Fig. 4. The top frame shows the maximum electron temperature, $T_e$, as a function of time. The bottom curve shows the kinetic energy in each of the first eight (8) toroidal harmonics during this time period. It is seen that as multiple modes become unstable and their kinetic energy peaks, the maximum $T_e$ begins to decrease. For the event shown, the $n = 4$ mode reaches the largest amplitude, and n = 2 persists, seemingly in a state of marginal stability. This is also the case for other crashes in this sequence and may be a consequence of the elongation.

The nonlinear calculations shown here were performed with the M3D-C1 code.[5,39] A time and space varying Spitzer resistivity profile was used, $\eta \sim T_e^{-3/2}$, but the resistivity was uniformly enhanced so that the central Lundquist number was $S = 10^6$. It used a uniform
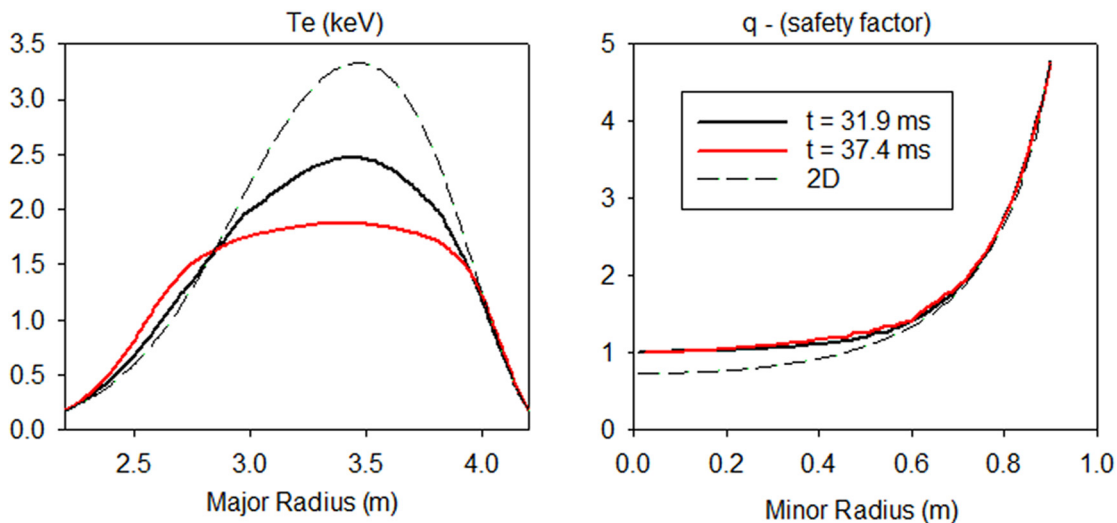


**FIG. 5.** (left) Temperatures along the midplane and (right) safety factor profile just before and just after sawtooth crash in Fig. 4. Also shown are the steady state results for a 2D (axisymmetric) calculation with the same heating and transport profiles.
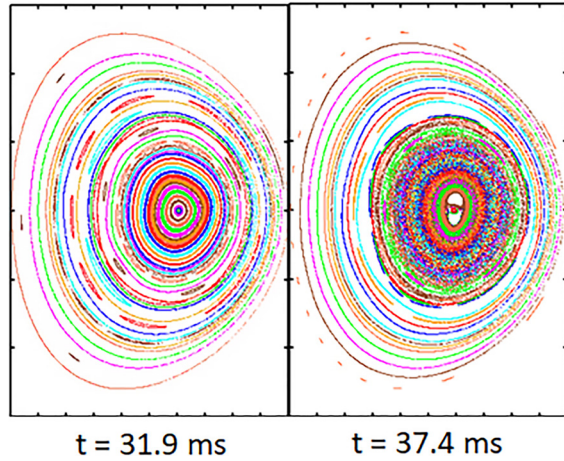
**FIG. 6.** Poincaré plots for the two times referred to in Fig. 5 for the calculation shown in Fig. 4.

viscosity with a value 10 times the central resistivity (dimensionless code units). The perpendicular thermal conductivity varied, increasing radially from 18 (center) to 36 (edge) times the central resistivity. The parallel thermal conductivity was $10^6$ times greater than the perpendicular one. Sufficient beam heating was applied to maintain $\beta$ at about 2.5%. The neutral beam model also drove a centrally peaked sheared toroidal velocity, which never exceeded 10% of the Alfvén velocity. A loop voltage was applied at the boundary in a feedback loop to keep the total toroidal current constant in time. The code uses a 3D finite element mesh. This calculation had 32 Hermite cubic finite elements in the toroidal direction and an unstructured mesh in the poloidal plane with 4th order Bell elements[40] of typical linear size 6 cm. This was a single-fluid simulation in which the temperature, density, and all components of the magnetic field were advanced. The calculation ran for $5 \times 10^5 \tau_A$ requiring $\approx 10^6$
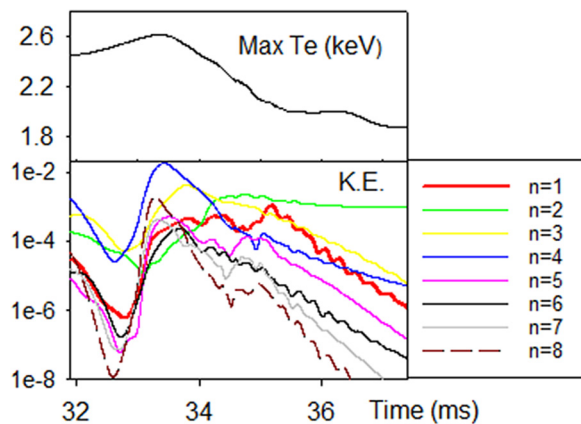


**FIG. 7.** Top: Close-up of maximum electron temperature (Max Te) in the region between dotted lines in Fig. 4. Bottom: Kinetic energy in the first 8 toroidal harmonics for the same time period. Note that the Max Te begins to decrease once the kinetic energy in several toroidal harmonics has peaked, creating a central stochastic region as shown in the right in Fig. 6.

processor-hours of computer time using 2.4 GHz Xeon processors with Infiniband interconnect.

Also shown in Fig. 1 is a schematic trajectory in the $(q_0, \beta_{p1})$ space of a sawtooth oscillation as calculated and depicted in Figs. 4–6. At location (A), the instability threshold for several $(m, n)$ modes with $m = n > 1$ is exceeded. As these modes grow, they locally increase the pressure gradient and excite other $(m, n)$ modes with $m = n > 1$. These many interchange modes destroy the surfaces in the center as shown on the right in Fig. 6, collapsing the central pressure without changing the $q$-profile as shown in Fig. 5. Once the central pressure is flattened (B), these modes become stable and the magnetic surfaces reform. As central heating is applied, the central pressure will again increase and $q_0$ will initially decrease due to resistive diffusion. Once the (1, 1) stability boundary is crossed (C), the associated central dynamo voltage will act to raise $q_0$ and stabilize its drop. When the increasing central pressure causes the stability threshold for several $(m, n)$ modes with $m = n > 1$ to be crossed again, the process will repeat.

Note that Fig. 1 is an idealized calculation of the linear stability with model $q$-profile and $p$-profile, circular cross-sectional axisymmetric plasmas. The actual nonlinear calculation depicted in Figs. 4–7 is more complex because it is non-circular geometry and because each of the unstable modes will deform the plasma column, affecting the linear stability of the other modes. We believe that the trajectory shown is qualitatively correct but not quantitatively. In addition, the stabilizing effect of sheared toroidal rotation present in the simulations and normally in the experiments was not taken into account.

### B. The relation to stationary states

Both the stationary state simulations presented in Refs. 11 and 29 and the sawtooth simulation in the present paper had $q_0$ slightly above 1 with low central shear. The primary differences were in the $\beta$ values and in the sheared rotation velocities. The stationary run in Ref. 29 had $\beta \simeq 2.0\%$ and central rotation velocity $V(0) \simeq 0.001 V_A$, decreasing to 0 at the edge. The sawtoothing run in this paper had slightly higher $\beta \simeq 2.5\%$ and central rotation velocity $V(0) \simeq 0.01 V_A$, about ten times larger. Clearly, many more runs need to be made in the future to determine the sensitivity to these and other parameters.

### V. MSE MAGNETIC SIGNATURE

Here, we illustrate what the magnetic signature of such interchange modes that flatten the pressure profile but leaves the $q$-profile unchanged might look like according to a motional Stark effect (MSE) diagnostic. We start with a toroidal equilibrium with a circular cross section, aspect ratio $R/a = 3.2$, minor radius $a = 1$ m, and a pressure profile and a $q$-profile given by Eqs. (1) and (2). Here, $\tilde{\psi}$ is the normalized poloidal magnetic flux, $\mu_0 p_0 = 0.02$ (SI units), $\psi_1 = 0.2$, $q_0 = 1.008$, $q_1 = 3.5322$. With a vacuum toroidal field at $R = 3.2$ m of 1 T, this equilibrium has $\beta = 2\langle p \rangle / \langle B^2 \rangle = 0.9675\%$. We designate this equilibrium as "before." We postulate that the final state is equilibrium with the same $q$-profile but with a pressure profile now given by

$$p = \begin{cases} p_1 & \text{if } \tilde{\psi} \le \psi_1 \\ p_0 \times (1 - \tilde{\psi})^2 & \text{if } \tilde{\psi} > \psi_2. \end{cases} \quad (3)$$

Here, $\psi_2 = 0.3$. In the interval $\psi_1 < \tilde{\psi} < \psi_2$, a cubic spline fit is used, which makes both $p$ and $dp/d\psi$ continuous. The value $p_1 = 0.0155$ makes $\beta$ for this "after" equilibrium the same as the "before"
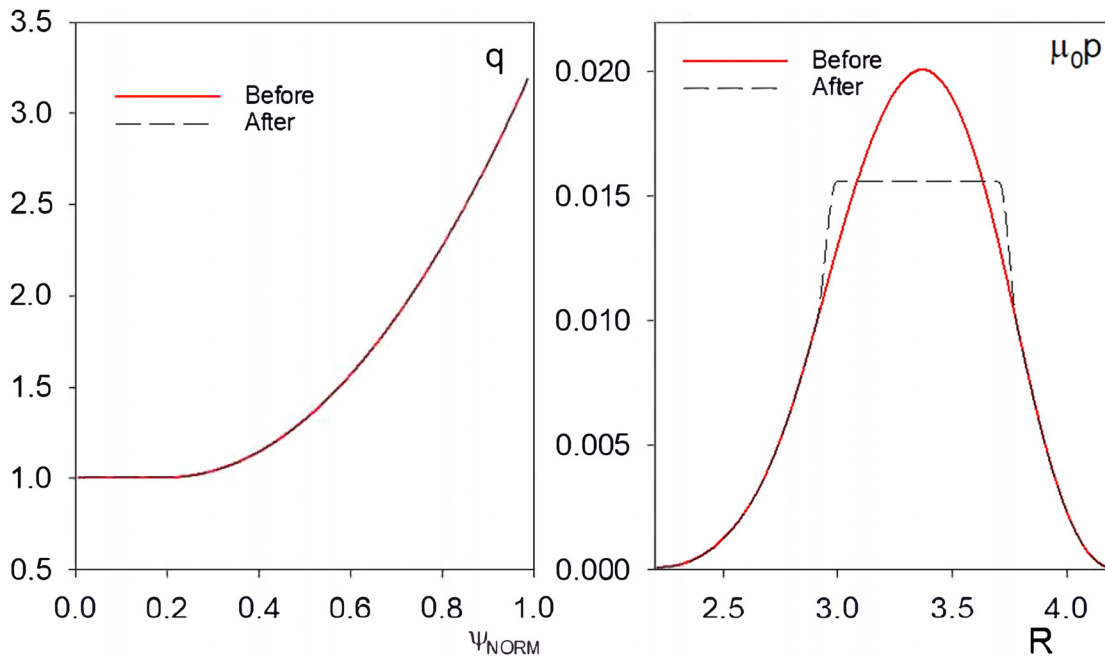
**FIG. 8.** (Left) Safety-factor ($q$) and (right) pressure ($\mu_0 p$) profiles used in the two equilibria.

equilibrium. These profiles are illustrated in Fig. 8. These high-accuracy equilibria were computed with the QSOLVER[41] inverse equilibrium code and verified with the M3D-C1 equilibrium option.

This second equilibrium is accessible since it has the same $q$-profile and stored energy as the first, although the pressure (and entropy) profiles have changed as a result of the interchange instability. This change led to a substantial change in the toroidal current profile as shown in Fig. 9.

Figure 10 shows a closeup of the flux surfaces in the central portion of the two equilibria. The magnetic axis has shifted from $R = 3.369\,4$ m to $R = 3.353\,8$ m. Also shown are vertical lines at 2 cm intervals in $R$, along which the ratio $\tan\gamma = B_Z/B_T$ is evaluated and plotted in Fig. 11. It is evident that despite the fact that the $q$-profile and $\beta$ values are identical for the two equilibria, the magnetic field at given $R$, $Z$ locations has changed substantially near the center of the discharge.

A commonly used formula for the safety factor at the magnetic axis, $R_{MA}$, is given by[42,43]

$$q_0 = \frac{\kappa}{R_{MA}} \left( \frac{\partial}{\partial R} \tan\gamma \right)^{-1}_{R=R_{MA}} . \qquad (4)$$

We compute the slopes of the 2 lines in Fig. 12 as 0.302 (before) and 0.306 (after). Using the boundary ellipticity of $\kappa = 1$ and evaluating Eq. (4) at the magnetic axis locations give $q_0 = 0.983$ (before) and $q_0 = 0.974$ (after). Comparing these with the true value, $q_0 = 1.008$, from the high-accuracy equilibrium code, we see that the before value is accurate to 2.4%, and the after value is off by about 3.3%.

In summary, in measuring the change (or lack of change) in $q_0$ during a sawtooth event with $q_0 \gtrsim 1$, it is clear from Fig. 11 that one

cannot rely on the change in $\tan\gamma = B_Z/B_T$ at a single radial position, which can be substantial. However, even with the exact value at multiple locations near the axis, the measurement uncertainty can easily be $2\% - 3\%$ or greater. This is in addition to the other known sources of error such as compensating for the radial electric field and subtraction
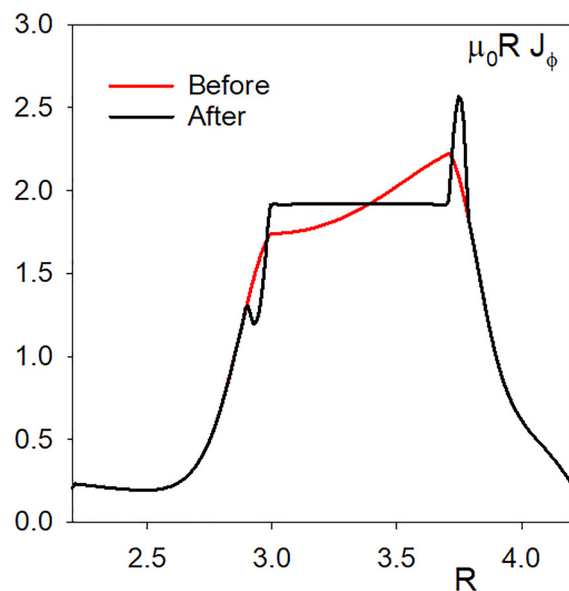


**FIG. 9.** Midplane current profiles, $\mu_0 R J_\phi$, for the two equilibria shown in Fig. 4.
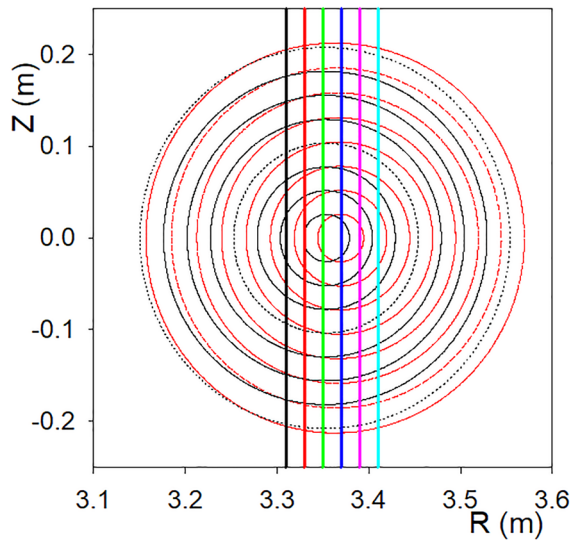
**FIG. 10.** Close-up of the change in central flux surfaces before and after the instability. The six vertical lines are at $R = 3.31$ m, 3.33 m, 3.35 m, 3.37 m, 3.39 m, and 3.41 m. Red curves denote "before equilibrium," and black curves denote "after."

of the background. The incorporation of an equilibrium reconstruction code such as EFIT[44] and/or a current diffusion calculation between sawteeth based on neo-classical resistivity[45] could help us to reduce this error, but they are subject to their own set of assumptions, which would need to be verified.

## VI. DISCUSSION

People have been performing computational studies of sawteeth for over 40 years.[7] Why has not this effect been observed before? Likely essential features for the computational model include (1) fully 3D MHD with many helical modes present, (2) full MHD equations (not reduced MHD), (3) toroidal geometry, (4) implicit time advance for long time simulations covering multiple sawtooth periods, and (5)
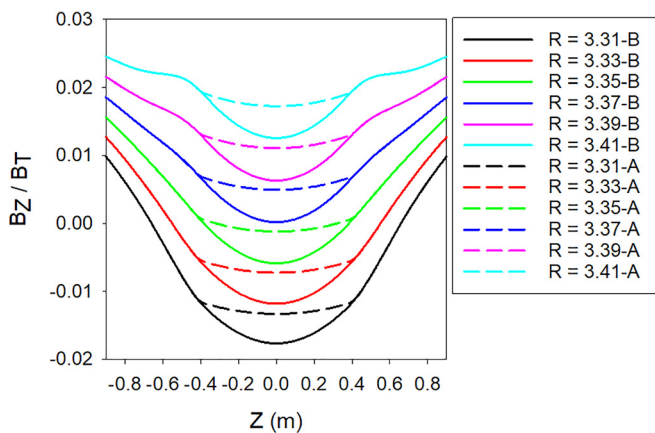


**FIG. 11.** Value of $\tan\gamma = B_Z/B_T$ along the six vertical lines shown in Fig. 10 for the two equilibria. Solid curves denote "before equilibrium," and dashed curves denote "after equilibrium."
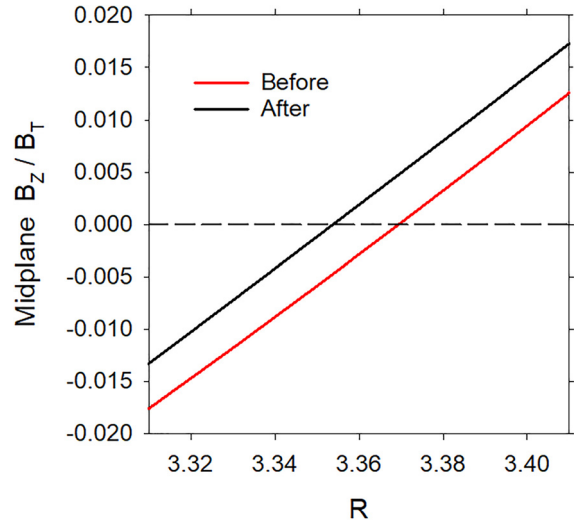


**FIG. 12.** Midplane values of the field ratio $\tan\gamma = B_Z/B_T$ as a function of the major radius for the "before" and "after" equilibrium.

high resolution, especially in the toroidal directions.[14] These features have only fairly recently been computationally feasible.

### A. Experimental results

The experimental measurement of the $q$-profile near the magnetic axis of a tokamak by the motional Stark effect (MSE) and other diagnostics is notoriously difficult. The value of $q_0$ is proportional to the flux surface average of the ratio of the toroidal magnetic field to the poloidal magnetic field in the limit as the latter vanishes at the axis. The intrinsic electric field due to ambipolar diffusion in the core must be taken into account, as must ellipticity in the core. Many teams have published the results of measuring the $q$-profile just before and after a sawtooth event with apparently conflicting results.

Early results by West[46] measured $q_0 = 0.7 \pm 0.05$, which increases as the edge $q$ increases on TEXT using the laser-induced fluorescence of an injected neutral Li beam. Soltwisch[47] measured an 8% change from 0.77 on TEXTOR (Ohmic with FIR). On PBX-M, $q_0$ was measured to be $0.63 \pm .03$ (MSE), $0.7 \pm 0.2$ (x-ray pinhole), and $0.8 \pm 0.14$ (fast ion diagnostic).[42] These early results of $q_0$ staying well below 1 in smaller tokamaks were also confirmed on JET and TFTR. Wolf[48] applied both FIR and MSE to JET and found that $q_0$ is in the range of $0.7 - 0.85$ throughout the sawtooth cycle. Yamada *et al.*[49] found that $q_0$ changed from 0.7 to 0.8 on TFTR. These measurements seemingly contradicted all prevailing theories, including the one presented here.

However, early measurements by Goldston analyzing fast ion orbits found $q_0$ to be clamped at 1 in ATC.[50] Wesson[26] quotes McCormick, on his experience on using Zeeman splitting of a lithium beam on ASDEX, as saying "it is found that when $q_0$ is lowered to unity, it shows a *resistance* to going below unity." The TEXT measurement referenced above was apparently contradicted by Wroblewski *et al.*[51] and Huang *et al.*[52] who quote a value very near unity for several discharges with differing edge-$q$, inferring a low shear central region, especially at low edge-$q$. Weisen *et al.*[53] used resonant Alfvén waves to deduce that TCA had a time-averaged $q$-profile with a flat central

region with $q_0$ close to unity. The JET result quoted above was seemingly at odds with Gill *et al.,*[54] analyzing x-ray emission when an injected pellet crosses the $q = 1$ surface, and found that the magnetic shear interior to the $q = 1$ surface was very low, making it difficult to reconcile with Ref. 48 Wroblewski[55] reported that $q_0$ in DIII-D is close to unity and the increase during the sawtooth crash is of order of the measurement error, 0.05. The analysis of BAE modes during a sawtooth crash on TORE SUPRA[56] implies that $q_0$ is normally slightly above unity before the sawtooth crash, typically ∼1.006, and decreases to unity after the crash. A recent study on KSTAR[57] supported by very high accuracy MSE measurements and supplemental MHD analysis concluded that $q_0$ was ∼1 in sawtoothing discharges with a relative accuracy of $\pm 0.03$ and with compelling evidence that it is slightly above 1 after the crash. These measurements of $q_0 \gtrsim 1$ before and after the crash are consistent with the model presented here.

There is also experimental soft x-ray evidence of a non-resonant (2, 2) mode appearing just before a sawtooth crash when a (1, 1) mode is also present in EAST.[58] In HT-7,[59] the tomography of high-resolution soft-x-ray emission led to the statement "that a purely fast reconnection of the $m = 1$ magnetic island is not responsible for the crash," and it emphasizes the importance of higher $m$ modes, especially (2, 2). The analysis of SXR signals on ASDEX-U[60] led to the conclusion that "…the sawtooth oscillations cannot be fully described by a single (1, 1) helicity. One has to include at least the second (2, 2) component before and after the crash. The small third component (3, 3) is also seen before the crash." These measurements of higher mode numbers during the crash appear to be consistent with the model presented here. Also, the present model has many features in common with the stochastic model of the sawtooth crash put forward by the ASDEX team.[61]

### B. Future work

The calculations presented here and in our previous work[11,29] were performed with a resistive MHD fluid model of the plasma,[5] which should be adequate to describe resistive diffusion and resistive and ideal MHD stability phenomena. The nonlinear calculations were also restricted to a configuration with a particular cross section shape as described in Sec. IV. It remains to be seen if the model presented here can be extended to describe such things as "monster sawteeth"[62,63] and the control of the sawtooth period by RF[64] and neutral beams.[64,65] Also, we have yet to demonstrate the dependence of the sawtooth period on the plasma shape[66] and other parameters. These studies and more detailed experimental validation, including the presence or absence of precursor and/or postcursor oscillations, will be the subject of future work.

### VII. CONCLUSIONS

In summary, our simulations indicate that sawtooth oscillations in tokamaks could be explained as follows: For sufficiently low-$\beta$ and low-$S$ discharges, the Kadomtsev model will apply. The temperature profile and current will peak, causing $q_0$ to fall below 1. A resistive (1, 1) mode will grow, flattening the temperature and density profiles interior to the $q = 1$ surface. However, above a critical value of $\beta$ and at sufficiently high $S$, a stationary (1, 1) interchange mode will grow and saturate, producing a dynamo voltage that keeps the central $q$-profile very close to 1 and flat due to a self-organizing feedback mechanism as described previously by us.[11,29] The saturated

interchange instability will also cause central flows that act to decrease the central pressure gradient through convection.

However, if the central heating is strong enough, the pressure in the low shear central region will continue to increase until higher-$n$ ideal modes, primarily with $m = n$, suddenly become unstable causing the central region to become turbulent and stochastic and the temperature and density to flatten. In this higher-$\beta$ centrally peaked heating regime, the role of the (1, 1) mode is to maintain the central $q$-profile very near 1 and the central region nearly shear-free. It is the higher $(m, n)$ ideal modes with $m = n > 1$ that cause the fast crash. We note here that since the temperature rise phase of the sawtooth period is due to heating and transport but the temperature crash phase is due to ideal MHD instabilities and parallel transport in stochastic fields, we expect the time separation between these two events to be even wider (and the crashes to be faster) as $S$ increases, and more realistic values of $\kappa_{||}$ are used.

The central features of our model are that in moderate-to-high $\beta$ tokamaks, (1) the $q$-profile remains just above unity with low central shear during the sawtooth and (2) higher-n modes are present during the crash. These are consistent with many experimental measurements, but they are in apparent conflict with others. More work clearly needs to be done to resolve these discrepancies.

### APPENDIX: ORIGIN OF THE DYNAMO VOLTAGE

The magnetic field in M3D-C1 is represented in the form

$$\mathbf{B} = \nabla \psi \times \nabla \varphi - \nabla_{\perp} \partial f / \partial \varphi + F \nabla \varphi, \qquad (A1)$$

where $F \equiv F_0 + \nabla_{\perp}^2 f$, with $F_0$ a constant. The poloidal velocity is represented as $\mathbf{V} = R^2 \nabla U \times \nabla \varphi + R^{-2} \nabla_{\perp} \chi$, a form of a Hodge decomposition. Here, $\nabla_{\perp}$ indicates the gradient perpendicular to the toroidal direction. In all the results presented here, the kinetic energy in the $\chi$ field is less than 1% of the energy in the $U$ field (which does not compress the strong toroidal magnetic field) and can thus be ignored in the analysis.

To the lowest order, the equation to advance the poloidal flux is given by[67]

$$\frac{\partial \psi}{\partial t} = R^2 [U, \psi] - \frac{\partial \Phi}{\partial \varphi} + \eta \Delta^* \psi. \qquad (A2)$$

Here, $(R, \varphi, Z)$ are cylindrical coordinates, $\Phi$ is the scalar electrical potential, and the Poisson bracket is defined in the normal way: $[a, b] = \nabla a \times \nabla b \cdot \nabla \varphi$.

As in Ref. 29 we note that a good fit to the (1, 1) component of the stream function is given by the unstable linear eigenfunction found in Ref. 27. For $r < r_1$,

$$U = U_0 r \left[ 1 - \left( \frac{r}{r_1} \right)^2 \right] \sin (\theta - \varphi). \tag{A3}$$

Here, $r$ is the minor radius, $r = |R - R_0|$, $r_1$ is the minor radius where the shear becomes non-zero, and $\theta$ is such that $(r, \theta)$ form a local polar coordinate system. Using the fact that to high order, $\nabla \Phi = -F \nabla U$, we can calculate the perturbed $\dot{\psi}$ field to the first two orders. To first order, $\dot{\psi}$ just has a (1, 1) component. Inserting Eq. (A3) into Eq. (A2) and just taking the (1, 1) component give, for $r < r_1$,

$$\dot{\psi}^{(1)} = \frac{1}{2} R^2 U_0 J_{\varphi 0} (1 - q_0) r \left[ 1 - \left( \frac{r}{r_1} \right)^2 \right] \cos (\theta - \varphi). \tag{A4}$$

Here, we defined the toroidal current density on axis as $J_{\varphi 0}$ and used the approximate identity $q_0 = 2F/(R^2 J_{\varphi 0})$. Inserting Eq. (A4) into Eq. (A2) gives for the second order contribution, for $r < r_1$,

$$\dot{\psi}^{(2)} = \frac{1}{2} R^2 U_0^2 J_{\varphi 0} (q_0 - 1) \left[ 1 - 3 \left( \frac{r}{r_1} \right)^2 \right] \left[ 1 - \left( \frac{r}{r_1} \right)^2 \right] - \eta R J_{\varphi 0}. \tag{A5}$$

Note that this second order (nonlinear) term is axisymmetric. It has the units of a voltage. Near the magnetic axis ($r = 0$), the first term is positive for $q_0 > 1$, while the second term, with the resistivity, is negative. The resistive term normally acts to lower the $q_0$ value, while the first term coming from the interchange instability acts to raise it. Since for a fixed pressure profile, the interchange growth rate and hence the magnitude of $U_0$ decrease quadratically with $(q_0 - 1)$ (see Fig. 2 of Ref. 27) a natural feedback mechanism is in place to keep $q_0$ slightly above 1.

## REFERENCES

[1] S. von Goeler, W. Studiek, and N. Sauthoff, Phys. Rev. Lett. **33**, 1201 (1974).
[2] F. Poli, Phys. Plasmas **25**, 055602 (2018).
[3] J. Wang, C. Xiao, X. Wang, X. Ji, and Y. Liu, Plasma Phys. Controlled Fusion **54**, 122001 (2012).
[4] A. Loarte, M. Reinke, A. Polevoi, M. Hosokawa, M. Chilenski, N. Howard, A. Hubbard, J. Hughes, J. Rice, J. Walk et al., Phys. Plasmas **22**, 056117 (2015).
[5] S. C. Jardin, N. Ferraro, J. Breslau, and J. Chen, Comput. Sci. Discovery **5**, 014002 (2012).
[6] Kadomtsev, B., Fiz. Plazmy **1**, 710 (1975) [Sov. J. Plasma Phys. **1**, 389 (1976)].
[7] A. Sykes and J. A. Wesson, Phys. Rev. Lett. **37**, 140 (1976).
[8] A. Y. Aydemir, J. C. Wiley, and D. W. Ross, Phys. Fluids B **1**, 774–787 (1989).
[9] F. D. Halpern, D. Leblond, H. Lutjens, and J. Luciani, Plasma Phys. Controlled Fusion **53**, 015011 (2011).
[10] W. Shen, G. Fu, Z. Sheng, J. Breslau, and F. Wang, Phys. Plasmas **21**, 092514 (2014).
[11] I. Krebs, S. C. Jardin, S. Guenter, K. Lackner, M. Hoelzl, E. Strumberger, and N. Ferraro, Phys. Plasmas **24**, 102511 (2017).
[12] W. Shen and F. Porcelli, Nucl. Fusion **58**, 106035 (2018).
[13] A. W. Edwards, D. J. Campbell, and W. W. Engelhardt, Phys. Rev. Lett. **57**, 210 (1986).
[14] A. Y. Aydemir, J. Y. Kim, B. H. Park, and J. Seol, Phys. Plasmas **22**, 032304 (2015).
[15] A. Y. Aydemir, Phys. Fluids B **2**, 2135 (1990).
[16] A. Y. Aydemir, Phys. Fluids B **4**, 3469 (1992).
[17] Q. Yu, S. Gunter, and K. Lackner, Nucl. Fusion **55**, 113008 (2015).
[18] M. Beidler, P. Cassak, S. Jardin, and N. Ferraro, Plasma Phys. Controlled Fusion **59**, 025007 (2017).
[19] Y. Nishimura, J. D. Callen, and C. Hegna, Phys. Plasmas **6**, 4685 (1999).
[20] S. Gunter, Q. Yu, K. Lackner, A. Bhattacharjee, and Y. Huang, Plasma Phys. Controlled Fusion **57**, 104017 (2015).
[21] L. Sugiyama, Phys. Plasmas **21**, 022510 (2014).
[22] B. Coppi, R. Galvao, R. Pellat, M. Rosenbluth, and P. Rutherford, J. Sov. Plasma Phys. **2**, 533 (1976).
[23] S. Hirshman and S. Jardin, Phys. Fluids **22**, 731 (1979).
[24] F. Porcelli, Phys. Rev. Lett. **66**, 425 (1991).
[25] J. Wesson, Plasma Phys. Controlled Fusion **28**, 243 (1986).
[26] J. Wesson, "Theory of sawtooth oscillations," in Proceedings of the Workshop on the Theory of Fusion Plasmas, Varenna, Italy 1987 (Editrice Compositori, Bologna, Italy, 1988).
[27] R. J. Hastie and T. C. Hender, Nucl. Fusion **28**, 585 (1988).
[28] F. L. Waelbroeck and R. D. Hazeltine, Phys. Fluids **31**, 1217 (1988).
[29] S. C. Jardin, N. Ferraro, and I. Krebs, Phys. Rev. Lett. **21**, 215001 (2015).
[30] C. Petty, M. E. Austin, C. T. Holcomb, R. Jayakumar, R. LaHaye, T. Luce, M. Makowski, P. Politzer, and M. Wade, Phys. Rev. Lett. **102**, 045005 (2009).
[31] A. Sips, R. Arslanbekov, C. Atanasiu, W. Becker, G. Becker, K. Behler, K. Behringer, A. Bergmann, R. Bilato, D. Bolshukhin et al., Plasma Phys. Controlled Fusion **44**, B69 (2002).
[32] N. Oyama, A. Isayama, G. Matsunaga, T. Suzuki, H. Takenaga, Y. Sakamoto, T. Nakano, Y. Kamada, S. Ide, and JT-60 Team, Nucl. Fusion **49**, 065026 (2009).
[33] E. Joffrin, F. Crisanti, R. Felton, X. Litaudon, D. Mazon, D. Moreau, L. Zabeo, R. Albanese, M. Ariola, D. Alves et al., Plasma Phys. Controlled Fusion **45**, A367–A383 (2003).
[34] P. Buratti, B. Alper, S. Annibaldi, A. Becoulet, P. Belo, J. Bucalossi, M. de Barr, P. de Vries, D. Frigione, C. Gormezano et al., Plasma Phys. Controlled Fusion **48**, 1005 (2006).
[35] J. Menard, R. Bell, D. Gates, S. Kaye, B. LeBlanc, F. Levinton, S. Medley, S. Sabbagh, D. Stutman, K. Tritz et al., Phys. Rev. Lett. **97**, 095002 (2006).
[36] I. Chapman, M. Hua, S. D. Pinches, R. Akers, A. Field, R. Hastie, C. Michael, and MAST Team, Nucl. Fusion **50**, 045007 (2010).
[37] L. Delgado-Aparicio, L. Sugiyama, R. Granetz, D. Gates, J. Rice, M. Reinke, M. Bitter, E. Fredrickson, C. Gao, M. Greenwald et al. Phys. Rev. Lett. **110**, 065006 (2013).
[38] P. Kirby, Nucl. Fusion **28**, 231 (1988).
[39] N. M. Ferraro, S. Jardin, M. Shephard, A. Bauer, J. Breslau, J. Chen, F. Delalondre, X. Luo, and F. Zhang, "Fluid modeling of fusion plasmas with M3D-C1," in Proceedings of the SciDAC 2011, Devner, CO, 10–14 July (2011).
[40] D. Braess, Finite Elements (Cambridge University Press, Cambridge, 2002).
[41] J. Delucia, S. Jardin, and A. Todd, J. Comput. Phys. **37**, 183 (1980).
[42] F. Levinton, R. Fonck, G. Gammel, R. Kaita, H. Kugel, E. Powell, and D. Roberts, Phys. Rev. Lett. **63**, 2060 (1989).
[43] J. Ko, Rev. Sci. Instrum. **87**, 11E541 (2016).
[44] L. Lao, H. St. John, and R. Stambaugh, Nucl. Fusion **25**, 1611 (1985).
[45] R. Fischer, A. Bock, A. Burckhart, O. Ford, L. Giannone, V. Igochine, M. Weiland, and M. Willensdorfer, and ASDEX Upgrade Team, Nucl. Fusion **59**, 056010 (2019).
[46] W. P. West, D. M. Thomas, J. S. DeGrassie, and S. Zheng, Phys. Rev. Lett. **58**, 2758 (1987).
[47] H. Soltwisch, Rev. Sci. Instrum. **59**, 1599 (1988).
[48] R. C. Wolf, J. Orourke, A. W. Edwards, and M. Vonhellermann, Nucl. Fusion **33**, 663 (1993).
[49] M. Yamada, F. Levinton, N. Pomphrey, R. Budny, J. Manickam, and Y. Nagayama, Phys. Plasmas **1**, 3269 (1994).
[50] R. Goldston, Phys. Fluids **21**, 2346 (1978).
[51] D. Wroblewski, L. Huang, H. W. Moos, and P. Phillips, Phys. Rev. Lett. **61**, 1724 (1988).
[52] L. K. Huang, M. Finkenthal, and D. Wroblewski, Phys. Fluids B **2**, 809 (1990).

[53]H. Weisen, G. Borg, B. Joye, A. Knight, and J. Lister, Phys. Rev. Lett. **62**, 434 (1989).

[54]R. Gill, A. Edwards, and A. Weller, Nucl. Fusion **29**, 821 (1989).

[55]D. Wroblewski and R. Snider, Phys. Rev. Lett. **71**, 859 (1993).

[56]C. Amador, R. Sabot, X. Garbet, Z. Guimaraes-Filho, and J. Ahn, Nucl. Fusion **58**, 016010 (2018).

[57]Y. B. Nam, J. S. Ko, G. H. Choe, Y. Bae, M. Choi, W. Lee, S. Jardin, and H. Park, Nucl. Fusion **58**, 066009 (2018).

[58]E. Li, V. Igochine, O. Dumbrajs, L. Xu, K. Chen, T. Shi, and L. Hu, Plasma Phys. Controlled Fusion **56**, 125016 (2014).

[59]Y. Sun, B. Wan, L. Hu, K. Chen, B. Shen, and J. Mao, Plasma Phys. Controlled Fusion **51**, 065001 (2009).

[60]V. Igochine, O. Dumbrajs, H. Zohm, A. Flaws, and ASDEX Upgrade Team, Nucl. Fusion **47**, 23 (2007).

[61]V. Igochine, J. Boom, I. Classen, O. Dumbrajs, s Gunter, K. Lackner, G. Pereverzev, H. Zohm, and ASDEX Upgrade Team, Phys. Plasmas **17**, 122506 (2010).

[62]S. Bernabei, M. Bell, R. Budny, E. Fredrickson, N. Gorelenkov, J. Hosea, R. Majeski, E. Mazzucato, C. Phillips, G. Schilling, and J. Wilson, Phys. Rev. Lett. **84**, 1212 (2000).

[63]L. Eriksson, A. Mueck, O. Sauter, S. Coda, M. Mantsinen, M. Mayoral, E. Westerhof, R. Buttery, D. McDonald, T. Johnson, J. Noterdaeme, and P. deVries, Phys. Rev. Lett. **92**, 235004–235001 (2004).

[64]I. Chapman, Plasma Phys. Controlled Fusion **53**, 013001 (2011).

[65]W. Heidbrink, E. Fredrickson, T. Mau, C. Petty, R. Pinsker, M. Porkolab, and B. Rice, Nucl. Fusion **39**, 1369 (1999).

[66]E. Lazarus, T. Luce, M. Austin, D. Brennan, K. Burrell, M. Chu, J. Ferron, A. Hyatt, J. Jayakumar, L. Lao *et al.*, Phys. Plasmas **44**, 055701 (2007).

[67]J. Breslau, N. Ferraro, and S. Jardin, Phys. Plasmas **16**, 092503 (2009).